Published in final edited form as:
Neuron. 2011 April 14; 70(1): 66–81. doi:10.1016/j.neuron.2011.03.008.

Muskelin Regulates Actin Filament- and Microtubule-Based $GABA_A$ Receptor Transport in Neurons

Frank F. Heisler[1], **Sven Loebrich**[1], **Yvonne Pechmann**[1], **Nikolaus Maier**[2], **Aleksandar R. Zivkovic**[2], **Mariko Tokito**[4], **Torben J. Hausrat**[1], **Michaela Schweizer**[1], **Robert Bähring**[3], **Erika L. F. Holzbaur**[4], **Dietmar Schmitz**[2], and **Matthias Kneussel**[1,5]

[1]Department of Molecular Neurogenetics, Center for Molecular Neurobiology, University of Hamburg Medical School, Germany

[2]Neuroscience Research Center, Charité-Universitätsmedizin Berlin

[3]Center for Experimental Medicine, University of Hamburg Medical School, Germany

[4]Department of Physiology, University of Pennsylvania, School of Medicine, Philadelphia, PA

Summary

Intracellular transport regulates protein turnover including endocytosis. Because of the spatial segregation of F-actin and microtubules, internalized cargo vesicles need to employ retrograde myosin and dynein motors to traverse both cytoskeletal compartments. Factors specifying cargo delivery across both tracks remain unknown.

We identified muskelin to interconnect retrograde F-actin- and microtubule-dependent $GABA_A$ receptor ($GABA_AR$) trafficking. $GABA_ARs$ regulate synaptic transmission, plasticity, and network oscillations. $GABA_AR$ α1 and muskelin interact directly, undergo neuronal cotransport, and associate with myosin VI or dynein motor complexes in subsequent steps of $GABA_AR$ endocytosis. Inhibition of either transport route selectively interferes with receptor internalization or degradation. Newly generated muskelin KO mice display depletion of both transport steps and a high-frequency ripple oscillation phenotype. A diluted coat color of muskelin KOs further suggests muskelin transport functions beyond neurons.

Our data suggest the concept that specific trafficking factors help cargoes to traverse both F-actin- and microtubule compartments, thereby regulating their fate.

Keywords

Neuron; Synapse; $GABA_A$ receptor; Muskelin; Dynein; Myosin; Transport; Motor protein; Internalization; OmniBank®; Lexicon; Cytoskeleton; Degradation; Oscillation

[5]Corresponding author: Prof. Dr. Matthias Kneussel Dept. of Molecular Neurogenetics Center for Molecular Neurobiology, ZMNH University of Hamburg Medical School Falkenried 94 D-20251 Hamburg Germany Tel. +49-40-74105-6275 Fax. +49-40-74105-7700 matthias.kneussel@zmnh.uni-hamburg.de.

Introduction

The delivery, removal and recycling of surface membrane proteins through cytoskeletal transport regulates a variety of cellular processes including cell adhesion and cellular signaling in various cell types (Hirokawa and Takemura, 2005; Soldati and Schliwa, 2006). Due to their polar and excitable nature, neurons represent cells with special requirements for transport. For instance, the rapid turnover of neurotransmitter receptors to and from postsynaptic membranes controls synaptic plasticity, the ability of individual synapses to change in strength (Kennedy and Ehlers, 2006; Nicoll and Schmitz, 2005).

Cytoskeletal transport is powered by molecular motor complexes that shuttle cargoes to specific subcellular compartments. A growing number of transport complexes have been functionally described in neurons (Caviston and Holzbaur, 2006; Hirokawa and Takemura, 2005; Soldati and Schliwa, 2006). However, the question of how cargo is guided across different cytoskeletal tracks to reach distinct subcellular destinations remains unanswered.

Myosins drive cargo along F-actin (Osterweil et al., 2005) and are thought to mediate local transport in proximity to the plasma membrane. In contrast, kinesin family proteins (KIFs) and dyneins use microtubules (MTs) as tracks for transport throughout the cell (Langford, 1995; Vale, 2003). Due to the nature of MT polarity in distal neurites (Baas et al., 1988), dyneins traffic cargoes mainly towards the cell center. With respect to their retrograde transport direction, dyneins and certain myosins have been implicated in endosomal sorting (Chibalina et al., 2007; Driskell et al., 2007).

The endocytic pathway consists of a network of spatially segregated sorting compartments that function to determine the cellular destination and fate of internalized cargo (Gruenberg and Stenmark, 2004; Soldati and Schliwa, 2006). Post internalization, cargo is transported to peripheral sorting endosomes, dynamic compartments where sorting decisions are made (Bonifacino and Rojas, 2006). In accordance to an enrichment of F-actin at the cellular cortex, transport across this region depends on myosin motor proteins (Neuhaus and Soldati, 2000; Osterweil et al., 2005). Individual transmembrane proteins can be recycled back to the plasma membrane, either directly or via the endocytic recycling compartment (ERC) (Traer et al., 2007). Alternatively, they undergo degradation at lysosomes (Kennedy and Ehlers, 2006) that are in close proximity to the nucleus and the MT-organizing center (Bonifacino and Rojas, 2006; Gruenberg and Stenmark, 2004). Consistent with this view, MT-dependent dynein motors participate in transport toward these organelles (Burkhardt et al., 1997; Driskell et al., 2007; Liang et al., 2004). Whether and to which extent F-actin- and MT-based transport processes overlap or share regulatory transport factors, is barely understood. However, cargo vesicles are thought to change drivers along the way and, consistent with this view, physical interactions between the F-actin- and MT-dependent motors MyoVA and KhcU have been reported (Huang et al., 1999).

$GABA_A$Rs mediate synaptic inhibition in the mammalian brain (Jacob et al., 2008). Functional receptors are expressed in a spatio-temporal manner and assemble as heteropentamers that consist of two α and two β subunits together with one subunit of either class, γ, δ, ε, θ or π (Jacob et al., 2008). $GABA_A$Rs are rapidly exchanged at neuronal surface membranes underlying the regulation of synaptic plasticity and network oscillation (Buzsaki and Draguhn, 2004; Jacob et al., 2008). Dysfunctions in GABAergic transmission contribute to a variety of neurological disorders (Mohler, 2006), however due to compensatory effects, mouse KOs of single receptor subunits only revealed marginal phenotypes (Sur et al., 2001). Surface $GABA_A$Rs undergo endocytosis and lysosomal degradation (Kittler et al., 2004), however except for AP2-clathrin complexes that mediate initial steps of internalization (Kittler et al., 2000) little is known about the molecular factors

that retrogradely drive $GABA_A$Rs toward vesicle compartments. Apart from dynein-based transport of glycine receptors (Maas et al., 2006), the detailed retrograde trafficking route of inhibitory neurotransmitter receptors remains elusive.

Here, we identified muskelin as a direct $GABA_A$R α1 subunit binding protein that participates in receptor endocytosis and degradation. Muskelin is a widely-expressed intracellular multidomain-protein (Adams et al., 2000; Adams et al., 1998), with high expression levels in hippocampus and cerebellum (Tagnaouti et al., 2007).

Our data show that muskelin accompanies receptor transport through different motor protein complexes along both actin filament and MT networks.

Results

$GABA_A$ receptors bind to and colocalize with muskelin

To identify $GABA_A$R binding proteins that might participate in the regulation of receptor targeting and/or turnover, we applied the LexA yeast two-hybrid system, using the intracellular $GABA_A$R α1 TMIII-TMIV loop sequence (aa 334–420, Figure 1A) as bait. From 2.4 million clones of an adult rat brain library, we identified five putative $GABA_A$R α1 binding partners including a single clone that coded for residues 90–200 of the multidomain protein muskelin (accession No. NM_031359), containing a discoidin domain, a lissencephaly-1 (LIS1) homology (LISH) and C-terminal to LisH (CTLH) tandem domain, as well as repeated kelch motifs (Adams et al., 1998) (Figure 1B). The muskelin binding site of $GABA_A$R α1 was mapped through TMIII-TMIV deletion mutants, which identified residues 399–420 as being sufficient for muskelin interaction (Figure 1A). Notably, TMIII-TMIV sequences of $GABA_A$R α2, α3, α5, β2 or γ2 subunits did not directly bind to muskelin in this assay (Figure 1C, D), while USP14 (a positive control) displayed binding (Supplemental Figure S5). To biochemically substantiate this interaction, we performed GST-pulldown and coimmunoprecipitation (co-IP) experiments. Despite $GABA_A$R α1, $GABA_A$R α2 TMIII-TMIV loop-GST fusion proteins also, but not GST alone or fusions to α3, α5, β2 or γ2, displayed specific binding to myc-muskelin derived from HEK293 cells (Figure 1E). $GABA_A$R α2 might associate with muskelin-$GABA_A$R α1 complexes, as it binds to gephyrin (Tretter et al., 2008), which can also interact with muskelin (Figures S1A and S1B); however, $GABA_A$R α2 does not seem to be a direct muskelin binding partner (Figures 1C and 1D).

Notably, as a control for muskelin-$GABA_A$R α1 binding, deletion of the minimal muskelin-binding motif of $GABA_A$R α1 (aa 399–420) abolished this interaction (Figure 1E). Accordingly, precipitation of endogenous $GABA_A$R α1 led to specific coprecipitation of endogenous muskelin and vice versa using brain lysates (Figure 1F, G). Coimmunostaining of hippocampal neurons, cultured for 12–14 days *in vitro* (DIV12–14) indicated colocalization of muskelin and $GABA_A$R α1 puncta in somata and neurites. Merged puncta were either positive or negative for the presynaptic terminal marker SV2, demonstrating both synaptic and non-synaptic colocalization, respectively (Figure 1H–J). Electron microscopy (EM) analysis of muskelin-specific immunoperoxidase signals confirmed this view. Muskelin was identified at post-, but not presynaptic sites, of many but not all symmetric (inhibitory) synapses (Figure 1K, L), as well as at individual nonsynaptic intracellular vesicles.

Genetic KO of muskelin in mice causes enhanced power of sharp wave-associated ripple oscillation

To investigate the biological role of muskelin, we established a muskelin KO mouse. Exon 1 of the *Mkln1* gene (encoding muskelin) encodes only 32 amino acids. An OmniBank® ES

cell clone (Zambrowicz et al., 1998) with an insertion of a retroviral gene trapping vector in intron 1 (primary RNA transcript: position 6970 bp) of the *Mkln1* locus (Figure 2A) was used. Heterozygous animals were crossed to produce WT (+/+), heterozygous (+/−), and homozygous (−/−) mice for further analysis. PCR and Southern blotting confirmed the presence of one mutant allele in +/− and two mutant alleles in −/− animals, respectively (Figure 2B and C). In addition, western blot analysis using a muskelin-specific antibody (Ledee et al., 2005), confirmed that muskelin protein levels were reduced by half in +/− and completely lost in −/−, as compared to +/+ genotypes (Figure 2D). Accordingly, immunohistochemistry revealed a loss of muskelin signals in −/−, as compared to +/+ cerebellar and hippocampal tissue slices (Figure 2E, F) and the use of a second and independent muskelin antibody (Tagnaouti et al., 2007), failed to coprecipitate muskelin from −/−, but not from +/+ mice (Figure 2G). We therefore conclude that muskelin expression is completely abolished in KO animals. Cresyl violett stainings revealed no gross histological abnormalities in KO brain tissue slices (Figure 2H), suggesting that muskelin plays no major roles in brain development or anatomical changes might be subtle.

Functional GABAergic synaptic transmission is essential for synchronizing the activity of neuronal networks giving rise to different sets of neuronal population rhythms in the hippocampus, *i.e.* theta-, gamma-, and ripple oscillations (Buzsaki and Draguhn, 2004). All these hippocampal rhythms have been implicated in processes underlying the temporary storage and successive consolidation of long-term memories (Buzsaki and Draguhn, 2004; Diekelmann and Born, 2010).

To assess the consequences of muskelin deficiency on the level of neuronal network synchronization, we analyzed sharp wave-associated ripples in acute hippocampal slices (Maier et al., 2003) from muskelin KO and control animals in area CA1 (Figure 2I, J). Spectral analysis of sharp wave-ripples displayed a robustly enhanced power component in the ripple frequency range (Figure 2K). The distribution of cumulated ripple power also showed a systematic shift to higher values in slices from muskelin KO animals compared to controls ($p=1.1\times10^{-316}$, Kolmogorov-Smirnov test; 18 slices from control and 12 slices from muskelin KO mice, respectively; Figure 2L). This result suggests an important contribution of muskelin in balancing GABAergic signalling that is relevant for the precise coordination of neuronal network mechanisms during high-frequency ripples.

Muskelin deficiency causes extrasynaptic surface membrane accumulation of $GABA_A$Rs

Since muskelin colocalized with $GABA_A$R α1 and in close proximity to synapses (Figure 1), we asked whether the observed oscillation phenotype was due to $GABA_A$R changes at the cellular level. A surface membrane-enriched (SE) brain fraction revealed an approximately 44% increase in $GABA_A$R α1 signal intensities in the muskelin-deficient (−/−) background, as compared to WT (+/+) controls (Figure 3A, B). A similar increase in receptor cell surface levels was observed by live cell immunostaining of cultured hippocampal neurons. In muskelin-deficient cells, $GABA_A$R α1 signals displayed both significantly higher signal intensities and covered larger cell surface areas (Figure 3C, D), whereas $GABA_A$R α2 or β2/3 signals only showed marginal alteration between the genotypes (see Supplemental Figure S1C–F). Notably, in addition to muskelin depletion, competitive overexpression of red fluorescent muskelin fusion protein (mRFP-muskelin) aa 90–200 harboring the $GABA_A$R α1-binding motif (Figure 1B), also caused increased $GABA_A$R α1 cell surface levels in HEK293 cells (Figure 3E, F). Thus, the critical role of muskelin in regulating $GABA_A$R α1 cell surface levels is mediated through the direct binding of both proteins and can be mimicked in a nonneuronal system.

Analysis of miniature inhibitory postsynaptic currents (mIPSCs) in cultured neurons (data not shown) or acute hippocampal slices (Figure 3G–J) revealed significant, however

marginal differences in amplitudes, whereas mIPSC frequencies were unaltered. Further decay time constants were significantly slower in KOs versus WT controls. Therefore, $GABA_AR$ α1 receptor levels at synapses are just slightly altered with no major presynaptic contribution.

This prompted us to quantify $GABA_AR$ α1 signal intensities and areas after coimmunostaining with presynaptic SV2 (Figure 3K–M). Consistent with our mIPSC analysis, synaptic $GABA_AR$ α1 levels (Figure 3K, yellow puncta) displayed just minor differences between WT (+/+) and muskelin KO (−/−) cells (Figure 3L), whereas extrasynaptic receptor levels (Figure 3K, green puncta in merged image) were strongly increased through muskelin deficiency (Figure 3M). Accordingly, muskelin signals were found at extrasynaptic putative coated pits by EM (Figure 3N), pointing to a role of muskelin in receptor internalization. These observations in neurons derived from muskelin KOs were neither due to changes in presynaptic terminals (Figure 3O), excitatory and inhibitory synapse numbers (Figure 3P, Q), or altered synaptic clustering (Supplemental Figure S1G, H). Thus, the previously observed increase in surface receptor levels (Figure 3A–D) mainly represents extrasynaptic $GABA_AR$ accumulations.

$GABA_AR$ α1 internalization requires muskelin, F-actin and myosin VI

To study the effect of muskelin depletion on $GABA_AR$ internalization, which is known to be clathrin-dependent (Kittler et al., 2000) and to occur outside of synapses (Bogdanov et al., 2006), we used a fluorescent receptor internalization assay after labeling of surface $GABA_AR$ α1 in living neurons. In this assay internalized receptors (red signals) appeared in a punctate putative vesicular fraction within the cytoplasm, while remaining surface receptors stained green (Figure 4A). Neurons from muskelin KOs displayed significantly decreased $GABA_AR$ α1 internalization rates, in both somata and neurite processes (Figure 4B), indicating that muskelin is critical for $GABA_AR$ endocytosis. Quantitative line-scan analysis detected reduced internal fluorescent intensities in −/− cells (red channel), whereas intensities of surface $GABA_AR$ α1 (green channels) showed larger peaks at border areas of KO neurons, representing the plasma membrane (Figure 4C, D; compare with Figure 3A–D). An independent assay, based on receptor surface biotinylation (Kittler et al., 2004), revealed approximately 50% reduced $GABA_AR$ α1 levels over 720 min, as compared to a loading control (Figure 4E, F). This decrease was prevented in the presence of the F-actin polymerization inhibitor cytochalasin D (Figure 4E, F), indicating that an intact F-actin cytoskeleton is a prerequisite for removal of $GABA_AR$ α1 from the neuronal surface.

We therefore asked whether the retrograde-directed F-actin motor myosin VI, important in AMPA-type glutamate receptor internalization (Osterweil et al., 2005), might be part of a $GABA_AR$ α1-muskelin complex and whether its function might be required for $GABA_AR$ α1 internalization. Notably, precipitation with a muskelin-specific antibody led to co-IP of myosin VI from WT (+/+), but not from muskelin KO-derived (−/−) brain lysate (Figure 4G). Furthermore, the use of either a myosin VI-specific or a $GABA_AR$ α1-specific antibody led to co-IP of myosin VI, muskelin or $GABA_AR$ α1, respectively (Figure 4H, I). The three binding partners also cofractionated at similar molarities during sucrose gradient centrifugation, both in the presence and absence of detergent (Supplemental Figure S2A, B). However, $GABA_AR$ α1-myosin VI interactions remained in the absence of muskelin (Supplemental Figure S2 C, D) and the muskelin-myosin VI association unlikely seems to be direct (Supplemental Figure S2 E, F), suggesting a larger $GABA_AR$ α1-muskelin-myosin VI complex, which may also involve other trafficking factors (Supplemental Figure S2G). Within this complex muskelin might share regulatory functions (Supplemental Figure S2H, I), rather than physically bridging a $GABA_AR$ α1-myosin VI interaction.

In order to assess a possible functional significance of these physical interactions, we aimed to interfere with F-actin-based myosin VI functions. To this end, we coexpressed $GABA_AR$ α1 and $GABA_AR$ β3 in the presence or absence of a dominant-negative myosin VI mutant (Osterweil et al., 2005) in HEK293 cells. Alternatively, we overexpressed the functional dynein inhibitor dynamitin-myc (Burkhardt et al., 1997), which impairs retrograde transport via MTs. Analysis of cell surface $GABA_AR$ α1 levels through a surface biotinylation experiment revealed a strong increase in plasma membrane receptors by interference with myosin VI function, however not by inhibition of dynein motor function (Figure 4J, K). Notably, the use of myosin VI-deficient mice (Snell`s waltzer mutants, sv/sv) revealed increased $GABA_AR$ α1 levels in surface membrane-enriched brain fractions (Figure 4L, M). These results could be confirmed through surface immunostaining of myosin VI-deficient neurons (Figure 4N–O). We therefore conclude that myosin VI is a strong candidate for a driver in the F-actin-dependent initial steps of $GABA_AR$ endocytosis.

$GABA_AR$ α1 intracellular transport requires muskelin and dynein

Consistent with a putative role of muskelin in retrograde-directed transport processes, we identified many particles of a mRFP-muskelin that migrated in neurite processes during time-lapse video microscopy (Figures 5A–D). Mobility characteristics were similar to active retrograde motor protein transport (Caviston and Holzbaur, 2006) (Figure 5A). The frequency of particle velocities peaked at two distinct values, suggesting that muskelin might be a component of different motor complexes (Figure 5B). In addition to particles moving in retrograde directions towards the cell body (Figure 5C), we observed retrogradely cotransported particles of mRFP-muskelin with GFP-$GABA_AR$ α1 (Figure 5D). Another indication that muskelin, which is widely expressed (Prag et al., 2007; Tagnaouti et al., 2007), may be critical in intracellular transport, was obtained from muskelin KO mice that underwent a coat color switch over time. Homozygous, but not heterozygous KOs developed brighter fur over several days, characterized by a dilute color (Figure 5E, F). Lightening of coat colors is often due to an altered distribution of melanosomes within skin melanocytes (Barral and Seabra, 2004). The trafficking of these pigment granules requires interplay of actin-dependent myosin transport with MT-dependent kinesin and dynein transport (Rodionov et al., 2003; Watabe et al., 2008). We therefore asked whether a muskelin-$GABA_AR$ association might also couple to dynein, representing the retrograde motor that acts downstream of myosin VI functions in powering transport from early endosomes onwards (Driskell et al., 2007; Traer et al., 2007). To this end, we performed co-IPs on brain lysate with antibodies specific for the essential dynein component dynein intermediate chain (DIC), muskelin, or $GABA_AR$ α1. We observed co-IP of DIC with a muskelin-specific antibody (Figure 6A) and co-IP of $GABA_AR$ α1 with a DIC-specific antibody (Figure 6B). Moreover, a $GABA_AR$ α1-specific antibody coprecipitated both muskelin and DIC (Figure 6C). This triple association of proteins could be further confirmed by co-IP from vesicle-enriched (VE) brain lysate fractions (Figure 6D) and sucrose gradient centrifugation (Supplemental Figure S3A, B). Mapping experiments revealed that the LisH/CTLH domain of muskelin directly interacts with an N-terminal motif unique to the dynein subunit DIC1A (Supplemental Figure S3C–F). Accordingly, retrograde-directed comigrating particles of mRFP-DIC (Lardong et al., 2009) and YFP-muskelin fusion proteins could be identified in neurite processes over time (Figure 6E). To functionally study a putative role of dynein in later steps of $GABA_AR$ α1 endocytosis, we employed mice that transgenically overexpress the functional dynein inhibitor dynamitin in the postnatal nervous system (LaMonte et al., 2002). Consistent with our results from dynamitin overexpression in HEK293 cells (Figure 4J, K), $GABA_AR$ α1 levels were not increased in surface-enriched (SE) fractions from transgenic brains, but vesicle-enriched (VE) fractions displayed a significant accumulation of $GABA_AR$ α1 at intracellular membranes (Figure 6F, G). Consistent with a direct muskelin-DIC interaction, DIC-specific antibodies coprecipitate

much less receptor from muskelin KO extracts (Figure 6H, I), indicating that muskelin physically connects $GABA_AR$ α1 with the dynein motor complex. Intriguingly, muskelin KO mice, such as dynamitin overexpressor mice (Figure 6F, G), also displayed increased $GABA_AR$ α1 levels at vesicle-enriched intracellular fractions (Figure 6J, K). Together, our combined results point to a dual role of muskelin: i.) in actin-based myosin VI transport underlying the initial steps of receptor internalization close to the plasma membrane, and ii.) in MT-based dynein transport of receptors downstream of the actin-myosin system.

Muskelin participates in $GABA_AR$ α1 targeting to late endosomes

We obtained evidence that muskelin associates with both early and late endosomes from sucrose gradient centrifugation and EM analysis. In vesicle-enriched brain lysate fractions, $GABA_AR$ α1 and muskelin cofractionated with the transferrin receptor and the late endosome marker Rab-7 (Figure 7A, B). Accordingly, muskelin immunoreactivity was found in association with individual small vesicles near surface membranes (Figure 7C, arrow) and with individual multivesicular bodies (Figure 7D, left). A kinetic analysis of late endosomes and/or lysosomes in neurite processes revealed that muskelin (−/−) neurons displayed a significantly reduced mobility, compared to (+/+) neurons (Figure 7E, F), suggesting that muskelin is a critical trafficking component of degradative routes. Total numbers of late endosomes and/or lysosomes remained similar in both genotypes (Figure 7G), implying normal biogenesis of the organelles analyzed. We therefore applied a previously described receptor degradation assay (Kittler et al., 2004) to monitor the reduction of $GABA_AR$ α1 levels over time. A decline in receptor signal intensities over 720 min could be prevented upon MT-depolymerization with nocodazole (Figure 7H, I, compare with Figure 4E, F). Therefore both intact F-actin and MTs seem to be required to drive $GABA_AR$ α1 toward endosomal and lysosomal compartments, respectively. To control whether this assay reflected receptor degradation we applied leupeptin, an inhibitor of several lysosomal proteases and found that the loss of receptors was prevented accordingly (Figure 7H, I). Final evidence that these processes require muskelin was obtained from comparing WT (+/+) and muskelin KO (−/−) neurons. Upon muskelin depletion, $GABA_AR$ α1 levels at timepoint 0 min were increased (Figure 7J, K, left), reflecting the previously identified cell surface accumulation (compare with Figure 3A–D). Notably, at timepoint 720 min muskelin-deficient neurons still displayed similar $GABA_AR$ α1 amounts as obtained at 0 min (Figure 7J, K, right), indicating that muskelin is a critical determinant in $GABA_AR$ α1 degradation (Figure 7L). Importantly, the unrelated AMPA receptor GluR1 subunit was still degraded normally under identical conditions (Supplemental Figure S4A, B), indicating that proteolytic functions of lysosomes generally remain normal in muskelin KO mice. We therefore conclude that impairment in late endosomal and lysosomal trafficking reflects the observed changes in $GABA_AR$ α1 degradation upon muskelin deficiency.

In summary, our data demonstrate that muskelin acts as a dual component with common functions in two subsequent internalization and degradation steps involving different cytoskeletal elements and motor proteins (Figure 8).

Discussion

In this study, we identified muskelin as a novel $GABA_AR$α1 subunit-interacting protein that regulates receptor endocytosis via motor proteins. Our data suggest that muskelin belongs to a novel set of transport factors that accompany cargo delivery across different subsequent cytoskeletal transport systems.

Muskelin represents a multidomain-protein, expressed in most tissues including the central nervous system (Adams et al., 1998; Prag et al., 2007; Tagnaouti et al., 2007). Muskelin harbors both, a central LisH/CTLH tandem domain, known to mediate dynein interactions in

other proteins and a C-terminal kelch repeat β-propeller implicated in actin interactions (Adams et al., 2000). Accordingly, muskelin localizes to F-actin at the cellular cortex together with its binding partner p39 (Ledee et al., 2005). Consistent with muskelin interacting with myosin VI, an association of p39 with non-muscle myosin essential light chain was reported (Ledee et al., 2007). In light of muskelin's dual motor association, it translocates into the nucleus, a process regulated by its LisH motif (Valiyaveettil et al., 2008). Furthermore, LisH motif-containing proteins were previously shown to participate in retrograde, dynein-dependent trafficking of degradative organelles (Liang et al., 2004).

Motor proteins that retrogradely transport $GABA_AR$s in neurons and remove these receptors from inhibitory shaft synapses have so far been unknown. The finding that myosin VI and dynein mediate subsequent steps of $GABA_AR$ trafficking functionally connects previous results, which have shown that AMPA receptor internalization employs myosin VI (Osterweil et al., 2005), while glycine receptor retrograde transport to the cell soma is dynein-dependent (Maas et al., 2006). Consistent with the observed role of dynein in intracellular $GABA_AR$ transport downstream of myosin VI in this study, dynein motor complexes promote the retrograde transport of EGF receptors (EGFRs) from sorting endosomes onwards (Driskell et al., 2007). $GABA_AR$ internalization and trafficking toward late endosomes and/or lysosomes therefore seems to involve two distinct subsequent transport processes.

To prove whether muskelin is essential for $GABA_A$ receptor trafficking and GABAergic transmission, we generated muskelin KO mice and found a phenotype with respect to receptor internalization and degradation at the cellular level. Moreover, as GABAergic transmission participates in the regulation of network oscillations (Buzsaki and Draguhn, 2004; Koniaris et al., 2010), which are critical for spatial memory consolidation (Girardeau et al., 2009), we analyzed hippocampal ripples as a functional readout parameter to assess consequences of muskelin KO on neuronal network levels (Maier et al., 2009). Indeed, we observed a marked increase in the power of sharp wave ripple oscillations in slices from muskelin KO mice. This finding, in line with our observation that decay times of miniature IPSCs are significantly prolonged, is consistent with the recent demonstration that zolpidem, a $GABA_AR$ agonist preferentially activating the α1 subunit, enhances ripple power *in vitro* (Koniaris et al., 2010). It can therefore be speculated that an increase of extrasynaptic $GABA_AR$ α1 subunits expressed on parvalbumin-expressing GABAergic basket cells (Baude et al., 2007), which are known to discharge at high rate during ripples (Klausberger et al., 2003), results in a more pronounced tonic inhibition of these cells with a consecutive disinhibition of target principal neurons and elevated ripple power. A comparable scenario has been described recently: reduced AMPAR-mediated excitation of CA1 basket interneurons (by genetically disrupting PV-DeltaGluR-A) also results in augmented ripples (Racz et al., 2009). Together, our electrophysiological results of enhanced ripples in muskelin KO mice along with the observed enrichment in surface $GABA_AR$ α1 levels suggest an important role of muskelin in the fine-tuning of hippocampal ripples, which have been demonstrated to be necessary for the formation of spatial memory traces (Girardeau et al., 2009).

In addition, the coat color phenotype of muskelin KO mice confirms muskelin's role in traffic regulation at a higher order level. Melanosomes are lysosome-related organelles that derive from early endosomal membranes and have become the best-studied model system for cooperation between actin- and MT-transport (Barral and Seabra, 2004; Soldati and Schliwa, 2006). The differential distribution of melanosomes, underlying the pigmentation of skin cells, requires a highly regulated interplay between MT-based kinesins/dyneins with F-actin-based myosins (Rodionov et al., 2003; Watabe et al., 2008). Functional roles of muskelin in neuronal $GABA_AR$ transport across both cytoskeletal systems, together with the

diluted coat color of muskelin KO mice suggest that muskelin may act at a critical interface in the regulation of actin filament and MT-based transport.

Notably, muskelin is upregulated under conditions of cerebellar ischemia (Dhodda et al., 2004), a pathological condition characterized by downregulation of surface membrane $GABA_A$Rs in neurons (Zhan et al., 2006). This correlation is in agreement with data in the present study and suggests that increased muskelin expression promotes intracellular transport underlying receptor internalization. Muskelin might therefore be a potential drug target to control neuronal receptor levels in this pathological condition.

Further understanding in the regulation of $GABA_A$R internalization and intracellular transport is of general interest with respect to synaptic plasticity, network oscillations and disease. Effective spatial learning of rats in eight-arm radial maze experiments was critically dependent on the integrity of hippocampal sharp wave ripple oscillations (Girardeau et al., 2009), indicating their role in transferring labile memories from hippocampus to neocortex for long-term storage. Based on our findings of altered ripples in muskelin KO mice, behavioural experiments with these animals may lead to novel insights into processes of memory consolidation during sleep.

In summary, muskelin seems to represent a key factor for the integrity of GABAergic transmission underlying higher order network functions. This phenotype is corroborated by the fact that muskelin plays a central role at the subcellular level by acting as a novel trafficking protein, regulating transport of $GABA_A$Rs and possibly other cargoes such as melanocytes along the F-actin and MT cytoskeleton.

Experimental Procedures

Additional experimental procedures are provided in the supplemental information.

Yeast-two-hybrid screening

The Matchmaker LexA Yeast Two-Hybrid system (Clontech, Heidelberg, Germany) and a rat brain cDNA library (Origene, Rockville, Maryland) were used for protein-protein interaction screening. Interaction of bait (pGilda) and prey (pJG4–5) fusions were assayed by activation of the LEU2 and lacZ reporter as previously described (Loebrich et al., 2006). Plasmid DNA of positive clones was recovered and inserts were analyzed by dideoxy sequencing.

GST-pulldown

For pulldown experiments, HEK293 cells were washed 24 h after transfection with PBS and harvested in 1ml PBS, supplemented with 1% Triton and 1mM PMSF. *E. coli* BL21 lysates were obtained by sonification and centrifugation at 10,000 × g for 30 min. Bacterial lysates were coupled to glutathione-sepharose beads (Amersham, Freiburg, Germany) for 3 h. The HEK293 lysate was applied to the beads for 10–12 h. Beads were washed and then boiled in SDS sample buffer.

Muskelin KO mice / PCR / Southern blotting

The *Mkln1* gene (mouse accession: NM_013791; chr6.31329008–31439638) was targeted in an OmniBank® 129/SvEv Embryonic Stem cell (ES) clone (OST448976) with the OmniBank® Gene Trapping vector VICTR 48+MTII (Lexicon Pharmaceuticals, Inc, The Woodlands, TX). The exact location of the insertion was determined by inverse PCR to position 6970 bp in intron 1 of the primary RNA transcript of the muskelin gene locus. Most gene trap vectors disrupt endogenous messages and create null alleles (Zambrowicz et al.,

1998). Blastocyst injections were performed at Lexicon Pharmaceuticals Inc. ES cells used for injection were 129SvEvBrd agouti. Resulting chimeras were bred to C57Bl/6 albino. Heterozygous mice were backcrossed to C57/129 hybrid agouti. For PCR genotyping of offspring mice, the forward and reverse primers (A + B) detect the WT allele. Primer A was used in combination with a gene trapping vector specific reverse primer (A + C) to amplify a mutation-specific product that contains 96 nucleotides of OmniBank® vector sequence. Oligonucleotide primers (A, 5′-AGCTACTTAAACCAAGTCAATGAGG-3`; B, 5`-CTCATATGGTCATTTCAATATAGAGC-3`; and C, 5`-ATAAACCCTCTTGCAG TTGCATC-3`) were used in an equimolar multiplex reaction to amplify corresponding *Mkln1* alleles on mouse chromosome 6. Cycling conditions were 94°C for 15 sec, 65°C for 30 sec (−1°C/cycle), 72°C for 40 sec (10 cycles) followed by 94°C for 15 sec, 55°C for 30 sec, and 72°C for 40 sec (30 cycles). To confirm the genetic manipulation, Southern blot analysis on *SacI* digested genomic DNA was performed. A radiolabeled probe was generated with primers A and B (desribed above). Digestion of amplified fragments with *BamHI* resulted in a probe specific to position 6697–6907 (Blast, NCBI) of the primary muskelin transcript upstream from the vector insertion site. Due to an additional vector *SacI* restriction site, the radiolabeled probe detects a 6.8 kb (KO) and 16.7 kb (WT) fragment.

Supplementary Material

Refer to Web version on PubMed Central for supplementary material.

Acknowledgments

We thank J. C. Adams for critical comments on the manuscript and for sharing unpublished information. We are grateful to P. Zelenka for providing a muskelin-specific antibody. We thank the members of the network grant DFG-FG885 and K. Duncan for technical help and critical comments. We also thank E. Kronberg and T. Grundmann for excellent help with animal housing. Supported by National Institutes of Health grant NINDS NS060698 to E.L.F.H. and by the University of Hamburg Medical School, DFG grants KN556/1-1, KN556/1-2, KN556/1-3, FG885-KN556/4-1, and FG885-KN556/4-2, the Chica and Heinz Schaller Foundation, and the Hamburg State Excellence Initiative: “Neurodapt” to M.K.

References

Adams J, Kelso R, Cooley L. The kelch repeat superfamily of proteins: propellers of cell function. Trends Cell Biol. 2000; 10:17–24. [PubMed: 10603472]

Adams JC, Seed B, Lawler J. Muskelin, a novel intracellular mediator of cell adhesive and cytoskeletal responses to thrombospondin-1. Embo J. 1998; 17:4964–4974. [PubMed: 9724633]

Baas PW, Deitch JS, Black MM, Banker GA. Polarity orientation of microtubules in hippocampal neurons: uniformity in the axon and nonuniformity in the dendrite. Proc Natl Acad Sci U S A. 1988; 85:8335–8339. [PubMed: 3054884]

Barral DC, Seabra MC. The melanosome as a model to study organelle motility in mammals. Pigment Cell Res. 2004; 17:111–118. [PubMed: 15016299]

Baude A, Bleasdale C, Dalezios Y, Somogyi P, Klausberger T. Immunoreactivity for the GABAA receptor alpha1 subunit, somatostatin and Connexin36 distinguishes axoaxonic, basket, and bistratified interneurons of the rat hippocampus. Cereb Cortex. 2007; 17:2094–2107. [PubMed: 17122364]

Bogdanov Y, Michels G, Armstrong-Gold C, Haydon PG, Lindstrom J, Pangalos M, Moss SJ. Synaptic GABAA receptors are directly recruited from their extrasynaptic counterparts. EMBO J. 2006; 25:4381–4389. [PubMed: 16946701]

Bonifacino JS, Rojas R. Retrograde transport from endosomes to the trans-Golgi network. Nat Rev Mol Cell Biol. 2006; 7:568–579. [PubMed: 16936697]

Burkhardt JK, Echeverri CJ, Nilsson T, Vallee RB. Overexpression of the dynamitin (p50) subunit of the dynactin complex disrupts dynein-dependent maintenance of membrane organelle distribution. J Cell Biol. 1997; 139:469–484. [PubMed: 9334349]

Buzsaki G, Draguhn A. Neuronal oscillations in cortical networks. Science. 2004; 304:1926–1929. [PubMed: 15218136]

Caviston JP, Holzbaur EL. Microtubule motors at the intersection of trafficking and transport. Trends Cell Biol. 2006; 16:530–537. [PubMed: 16938456]

Chibalina MV, Seaman MN, Miller CC, Kendrick-Jones J, Buss F. Myosin VI and its interacting protein LMTK2 regulate tubule formation and transport to the endocytic recycling compartment. J Cell Sci. 2007; 120:4278–4288. [PubMed: 18029400]

Dhodda VK, Sailor KA, Bowen KK, Vemuganti R. Putative endogenous mediators of preconditioning-induced ischemic tolerance in rat brain identified by genomic and proteomic analysis. J Neurochem. 2004; 89:73–89. [PubMed: 15030391]

Diekelmann S, Born J. The memory function of sleep. Nat Rev Neurosci. 2010; 11:114–126. [PubMed: 20046194]

Driskell OJ, Mironov A, Allan VJ, Woodman PG. Dynein is required for receptor sorting and the morphogenesis of early endosomes. Nat Cell Biol. 2007; 9:113–120. [PubMed: 17173037]

Girardeau G, Benchenane K, Wiener SI, Buzsaki G, Zugaro MB. Selective suppression of hippocampal ripples impairs spatial memory. Nat Neurosci. 2009; 12:1222–1223. [PubMed: 19749750]

Gruenberg J, Stenmark H. The biogenesis of multivesicular endosomes. Nat Rev Mol Cell Biol. 2004; 5:317–323. [PubMed: 15071556]

Hirokawa N, Takemura R. Molecular motors and mechanisms of directional transport in neurons. Nat Rev Neurosci. 2005; 6:201–214. [PubMed: 15711600]

Huang JD, Brady ST, Richards BW, Stenolen D, Resau JH, Copeland NG, Jenkins NA. Direct interaction of microtubule- and actin-based transport motors. Nature. 1999; 397:267–270. [PubMed: 9930703]

Jacob TC, Moss SJ, Jurd R. GABA(A) receptor trafficking and its role in the dynamic modulation of neuronal inhibition. Nat Rev Neurosci. 2008; 9:331–343. [PubMed: 18382465]

Kennedy MJ, Ehlers MD. Organelles and trafficking machinery for postsynaptic plasticity. Annu Rev Neurosci. 2006; 29:325–362. [PubMed: 16776589]

Kittler JT, Delmas P, Jovanovic JN, Brown DA, Smart TG, Moss SJ. Constitutive endocytosis of GABAA receptors by an association with the adaptin AP2 complex modulates inhibitory synaptic currents in hippocampal neurons. J Neurosci. 2000; 20:7972–7977. [PubMed: 11050117]

Kittler JT, Thomas P, Tretter V, Bogdanov YD, Haucke V, Smart TG, Moss SJ. Huntingtin-associated protein 1 regulates inhibitory synaptic transmission by modulating gamma-aminobutyric acid type A receptor membrane trafficking. Proc Natl Acad Sci U S A. 2004; 101:12736–12741. [PubMed: 15310851]

Klausberger T, Magill PJ, Marton LF, Roberts JD, Cobden PM, Buzsaki G, Somogyi P. Brain-state- and cell-type-specific firing of hippocampal interneurons in vivo. Nature. 2003; 421:844–848. [PubMed: 12594513]

Koniaris E, Drimala P, Sotiriou E, Papatheodoropoulos C. Different effects of zolpidem and diazepam on hippocampal sharp wave-ripple activity in vitro. Neuroscience. 2010

LaMonte BH, Wallace KE, Holloway BA, Shelly SS, Ascano J, Tokito M, Van Winkle T, Howland DS, Holzbaur EL. Disruption of dynein/dynactin inhibits axonal transport in motor neurons causing late-onset progressive degeneration. Neuron. 2002; 34:715–727. [PubMed: 12062019]

Langford GM. Actin- and microtubule-dependent organelle motors: interrelationships between the two motility systems. Curr Opin Cell Biol. 1995; 7:82–88. [PubMed: 7755993]

Lardong K, Maas C, Kneussel M. Neuronal depolarization modifies motor protein mobility. Neuroscience. 2009; 160:1–5. [PubMed: 19250960]

Ledee DR, Gao CY, Seth R, Fariss RN, Tripathi BK, Zelenka PS. A specific interaction between muskelin and the cyclin-dependent kinase 5 activator p39 promotes peripheral localization of muskelin. J Biol Chem. 2005; 280:21376–21383. [PubMed: 15797862]

Ledee DR, Tripathi BK, Zelenka PS. The CDK5 activator, p39, binds specifically to myosin essential light chain. Biochem Biophys Res Commun. 2007; 354:1034–1039. [PubMed: 17276406]

Liang Y, Yu W, Li Y, Yang Z, Yan X, Huang Q, Zhu X. Nudel functions in membrane traffic mainly through association with Lis1 and cytoplasmic dynein. J Cell Biol. 2004; 164:557–566. [PubMed: 14970193]

Loebrich S, Bahring R, Katsuno T, Tsukita S, Kneussel M. Activated radixin is essential for GABAA receptor alpha5 subunit anchoring at the actin cytoskeleton. Embo J. 2006; 25:987–999. [PubMed: 16467845]

Maas C, Tagnaouti N, Loebrich S, Behrend B, Lappe-Siefke C, Kneussel M. Neuronal cotransport of glycine receptor and the scaffold protein gephyrin. J Cell Biol. 2006; 172:441–451. [PubMed: 16449194]

Maier N, Morris G, Johenning FW, Schmitz D. An approach for reliably investigating hippocampal sharp wave-ripples in vitro. PLoS One. 2009; 4:e6925. [PubMed: 19738897]

Maier N, Nimmrich V, Draguhn A. Cellular and network mechanisms underlying spontaneous sharp wave-ripple complexes in mouse hippocampal slices. J Physiol. 2003; 550:873–887. [PubMed: 12807984]

Mohler H. GABAA receptors in central nervous system disease: anxiety, epilepsy, and insomnia. J Recept Signal Transduct Res. 2006; 26:731–740. [PubMed: 17118808]

Neuhaus EM, Soldati T. A myosin I is involved in membrane recycling from early endosomes. J Cell Biol. 2000; 150:1013–1026. [PubMed: 10973992]

Nicoll RA, Schmitz D. Synaptic plasticity at hippocampal mossy fibre synapses. Nat Rev Neurosci. 2005; 6:863–876. [PubMed: 16261180]

Osterweil E, Wells DG, Mooseker MS. A role for myosin VI in postsynaptic structure and glutamate receptor endocytosis. J Cell Biol. 2005; 168:329–338. [PubMed: 15657400]

Prag S, De Arcangelis A, Georges-Labouesse E, Adams JC. Regulation of post-translational modifications of muskelin by protein kinase C. Int J Biochem Cell Biol. 2007; 39:366–378. [PubMed: 17049906]

Racz A, Ponomarenko AA, Fuchs EC, Monyer H. Augmented hippocampal ripple oscillations in mice with reduced fast excitation onto parvalbumin-positive cells. J Neurosci. 2009; 29:2563–2568. [PubMed: 19244531]

Rodionov V, Yi J, Kashina A, Oladipo A, Gross SP. Switching between microtubule- and actin-based transport systems in melanophores is controlled by cAMP levels. Curr Biol. 2003; 13:1837–1847. [PubMed: 14588239]

Soldati T, Schliwa M. Powering membrane traffic in endocytosis and recycling. Nat Rev Mol Cell Biol. 2006; 7:897–908. [PubMed: 17139330]

Sur C, Wafford KA, Reynolds DS, Hadingham KL, Bromidge F, Macaulay A, Collinson N, O'Meara G, Howell O, Newman R. Loss of the major GABA(A) receptor subtype in the brain is not lethal in mice. J Neurosci. 2001; 21:3409–3418. [PubMed: 11331371]

Tagnaouti N, Loebrich S, Heisler F, Pechmann Y, Fehr S, De Arcangelis A, Georges-Labouesse E, Adams JC, Kneussel M. Neuronal expression of muskelin in the rodent central nervous system. BMC Neurosci. 2007; 8:28. [PubMed: 17474996]

Traer CJ, Rutherford AC, Palmer KJ, Wassmer T, Oakley J, Attar N, Carlton JG, Kremerskothen J, Stephens DJ, Cullen PJ. SNX4 coordinates endosomal sorting of TfnR with dynein-mediated transport into the endocytic recycling compartment. Nat Cell Biol. 2007; 9:1370–1380. [PubMed: 17994011]

Tretter V, Jacob TC, Mukherjee J, Fritschy JM, Pangalos MN, Moss SJ. The clustering of GABA(A) receptor subtypes at inhibitory synapses is facilitated via the direct binding of receptor alpha 2 subunits to gephyrin. J Neurosci. 2008; 28:1356–1365. [PubMed: 18256255]

Vale RD. The molecular motor toolbox for intracellular transport. Cell. 2003; 112:467–480. [PubMed: 12600311]

Valiyaveettil M, Bentley AA, Gursahaney P, Hussien R, Chakravarti R, Kureishy N, Prag S, Adams JC. Novel role of the muskelin-RanBP9 complex as a nucleocytoplasmic mediator of cell morphology regulation. J Cell Biol. 2008; 182:727–739. [PubMed: 18710924]

Watabe H, Valencia JC, Le Pape E, Yamaguchi Y, Nakamura M, Rouzaud F, Hoashi T, Kawa Y, Mizoguchi M, Hearing VJ. Involvement of dynein and spectrin with early melanosome transport and melanosomal protein trafficking. J Invest Dermatol. 2008; 128:162–174. [PubMed: 17687388]

Zambrowicz BP, Friedrich GA, Buxton EC, Lilleberg SL, Person C, Sands AT. Disruption and sequence identification of 2,000 genes in mouse embryonic stem cells. Nature. 1998; 392:608–611. [PubMed: 9560157]

Zhan RZ, Nadler JV, Schwartz-Bloom RD. Depressed responses to applied and synaptically-released GABA in CA1 pyramidal cells, but not in CA1 interneurons, after transient forebrain ischemia. J Cereb Blood Flow Metab. 2006; 26:112–124. [PubMed: 15959457]

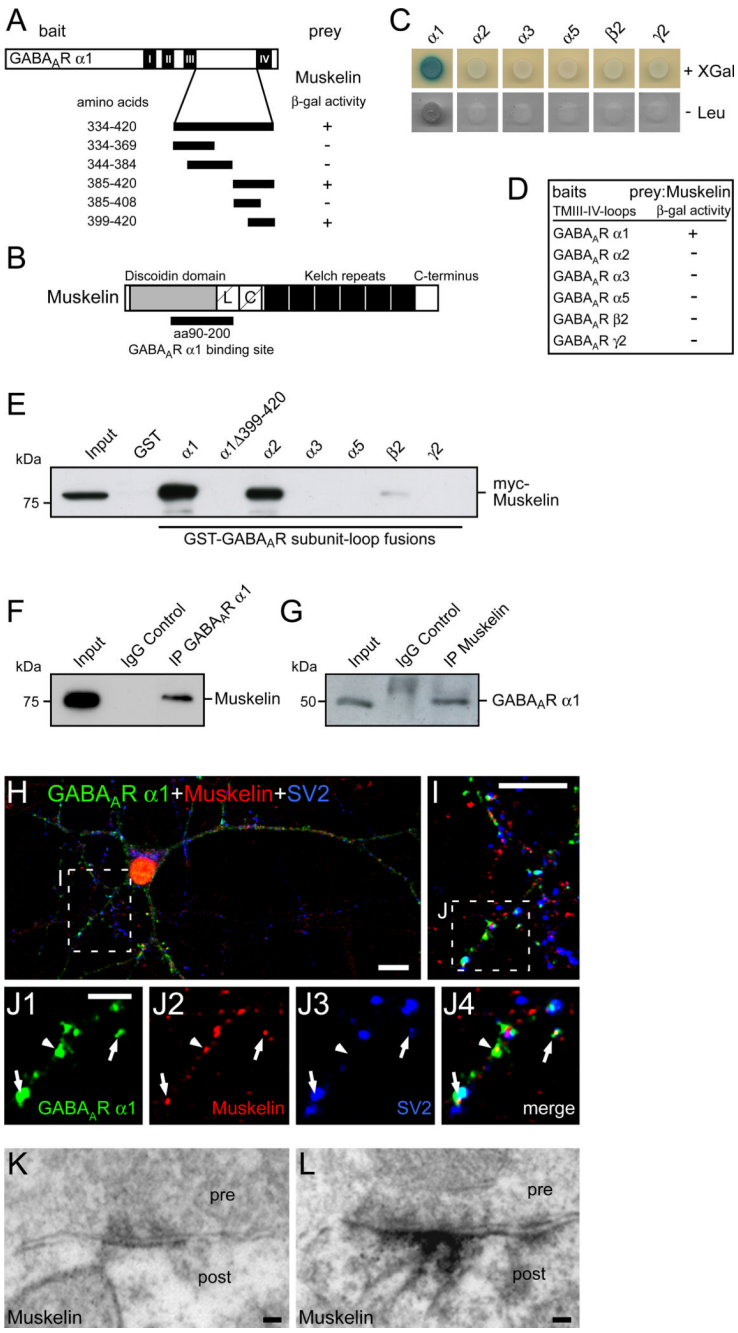

Figure 1. Direct interaction of muskelin with GABA$_A$R α1

(**A**) Scheme of GABA$_A$R α1 domain architecture. Sequences between transmembrane domains (TMs) III and IV were used for yeast-two hybrid screening. Deletion mutants were generated to map the muskelin binding motif. (+) indicates binding, (−) indicates no binding. (**B**) Scheme of muskelin domain architecture. The region indicated (black bar) was identified in the prey vector (**C, D**) lacZ gene expression and growth on leucin-deficient medium is induced through binding of muskelin to GABA$_A$R α1, but not to other GABA$_A$R subunit TM III–IV loops (C). (+) indicates strong binding and (−) indicates no binding (D). (**E**) GST-pulldown assay using different GABA$_A$R subunit TM III–IV-loops, fused to GST or a GABA$_A$R α1 TM III–IV-loop lacking the muskelin-binding motif (aa 399–420), fused

to GST. (**F**) Coimmunoprecipitation (co-IP) with $GABA_AR$ α1-specific antibodies coprecipitates muskelin from brain lysate. (G) co-IP with muskelin-specific antibodies coprecipitates $GABA_AR$ α1 from brain lysate. (**H–J**) Immunostaining in cultured hippocampal neurons displays colocalization of $GABA_AR$ α1 and muskelin signals at SV2-negative non-synaptic sites (arrowheads). Some overlapping signals colocalize with SV2 indicating synaptic localization (arrows). Boxed regions are shown at higher magnification. Scale bars: 20 μm (H, I); 5 μm (J). (**K, L**) Electron microscopy analysis of hippocampal tissue slices upon detection of DAB signals. Muskelin immunoreactivity labels postsynaptic but not presynaptic regions of many, but not all symmetric synapses. A muskelin-negative synapse is shown in (K); a muskelin-positive synapse is shown in (L). Signals are found in direct apposition with plasma membranes and at subsynaptic regions. Scale bars: 0.1 μm.

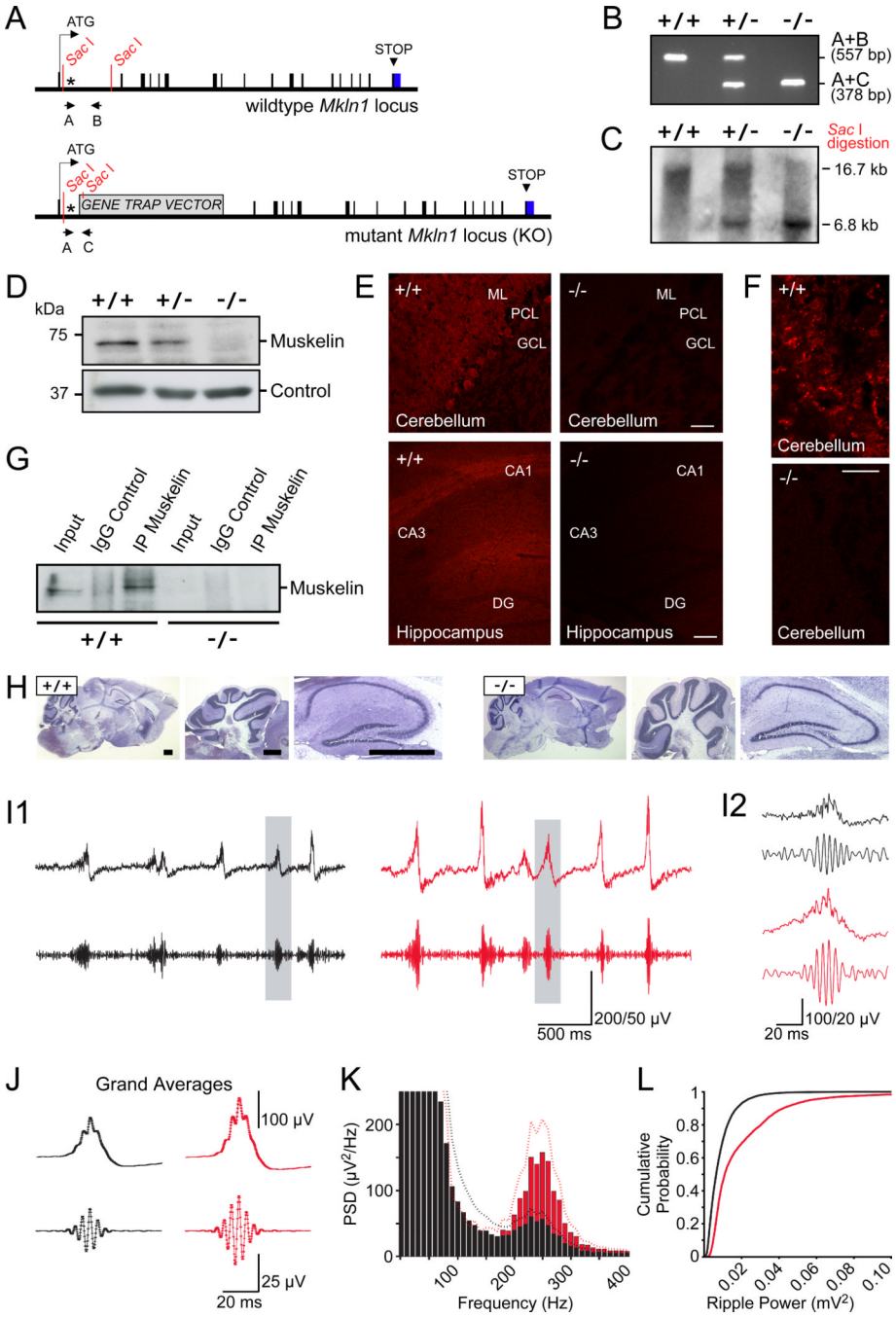

Figure 2. Generation of muskelin KO mice alters hippocampal network oscillations

(**A**) WT and mutant *Mkln1* gene locus (encoding muskelin). Black boxes represent exons, blue boxes untranslated regions. Intron 1 of mutant *Mkln1* harbours an inserted gene trap vector containing stop codons. *Sac I* restriction sites and *Mkln1*-specific probes (asterisks) were used for Southern blotting, primers A–C for PCR genotyping. (**B**) PCR genotyping. WT alleles: 557 bp band, mutant alleles: 378 bp band. (**C**) Southern blot genotyping. WT alleles: 16.7 kb band, mutant alleles: 6.8 kb band. (**D**) Western blot detection using muskelin-specific antibodies. Signal intensity is reduced in brain lysates from heterozygous (+/−) and lost in homozygous (−/−) mice. Control: Actin detection. (**E, F**) Immunohistochemistry on cerebellar and hippocampal tissue slices. Muskelin-specific

signals are detected in WT (+/+) and abolished in KO-derived (−/−) tissue (E). The loss of immunoreactive signals is more obvious at higher magnification of cerebellar neurons, known to express highest muskelin levels in brain (F). Scale bars: 150 μm (E) and 50 μm (F). (**G**) Muskelin-specific antibodies precipitate muskelin from WT (+/+) but not from KO (−/−) lysate. (**H**) Cresyl violett stainings reveal no gross histological abnormalities in KO (−/−) as compared to WT (+/+) brains. Cerebellum and hippocampus are shown at higher magnification. Scale bars: 1 mm. **(I)** Spontaneous neuronal network activity in hippocampal slices from control- (black) and muskelin KO mice (red). (**I1**) Representative example sharp waves and associated high-frequency ripples (upper traces) were recorded from area CA1b pyramidal cell layer. Bottom panels display the 150–300 Hz band pass-filtered versions of the above to isolate the oscillatory ripple component. Note that events from the muskelin KO slice, on average, display larger amplitudes. **(I2)** Magnification of the periods highlighted (grey boxes). **(J)** Grand averages representing 11,387 and 7,217 events from control and KO slices, respectively. Filter parameters as above. **(K)** Averages of power spectral density (PSD) functions from 21 control- and 12 KO slices. Ripple power at ~250 Hz is markedly enhanced in slices from muskelin KO animals. Dashed lines indicate SEM. **(L)** Cumulative distribution plots summarizing the population analysis on ripple power. Note the consistently increased values derived from muskelin KO slices (medians for KO and control: 0.011 mV^2 versus 0.007 mV^2; P : 0.007 mV^2 versus 0.004 mV^2 25 ; P_{75}: 0.025 versus 0.011).

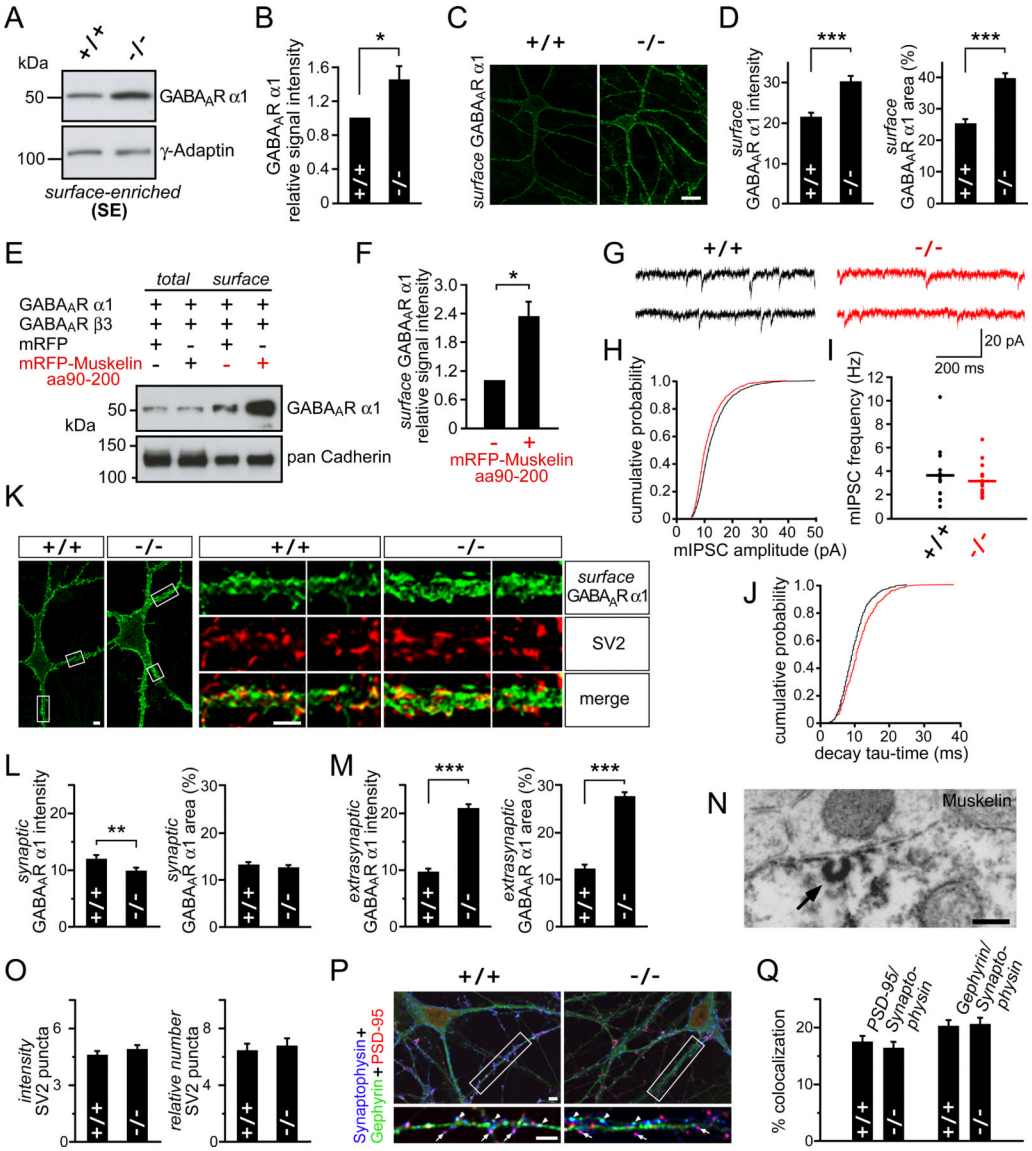

Figure 3. Muskelin depletion causes increased GABA$_A$R α1 surface levels with accumulation at extrasynaptic sites

(A, B) Increased GABA$_A$R α1 levels in surface-enriched brain lysate (SE) fractions upon muskelin depletion (−/−, 1.44±0.15) as compared to WT (+/+, set to 1) (n=7). Control: γ-adaptin detection. **(C, D)** Surface GABA$_A$R α1 immunostainings of hippocampal neurons. Dendritic GABA$_A$R α1 intensities and areas are significantly increased in muskelin depleted (−/−, 30.28±1.09 and 39.75±0.98) as compared to WT neurons (+/+, 21.52±0.80 and 25.34±0.73) (n=54 cells from three cultures of each genotype). Scale bar: 25 μm. **(E–F)** Analysis of GABA$_A$R surface biotinylation upon expression of GABA$_A$R α1 and GABA$_A$R β3 in HEK293 cells. Competitive interference with GABA$_A$R α1-muskelin direct binding through the isolated binding motif mRFP-muskelin (aa 90–200) causes increased GABA$_A$R α1 surface levels. mRFP(−) set to 1; mRFP-muskelin aa 90–200 (+), 2.34±0.28, n=3. **(G–J)** GABAergic transmission in WT (+/+, black) and muskelin depleted (−/−, red) pyramidal neurons. Miniature inhibitory postsynaptic currents (mIPSCs) were measured from brain slices. **(H)** Small shift in mIPSC amplitude distribution obtained from muskelin depleted (red, mean amplitude 11.7±0.1 pA) as compared to WT neurons (black, 13.1±0.2 pA) (n=16,

p<0.0001, Mann-Whitney U test). **(I)** Scatter plot showing mIPSC frequencies. Data points represent results from individual cells. Horizontal bars are mean values of WT (+/+, 3.6±0.6 Hz, n=16) and muskelin depleted neurons (−/−, 3.1±0.4 Hz, n=15, p=0.56, Mann-Whitney U test). (J) Significant shift in the distribution of mIPSC mean decay time constants in muskelin-deficient neurons (red, mean decay 11.4±0.2 ms), as compared to WT neurons (black, 9.9±0.1 ms) (n=16, p<0.001, Mann-Whitney U test).
(K–M) Immunostaining of surface $GABA_AR$ α1 and SV2 in cultured hippocampal neurons. Upon muskelin depletion $GABA_AR$ α1 accumulate at SV2-negative sites indicating extrasynaptic surface localization (n=54 cells from three cultures of each genotype). Boxed regions at higher magnification, scale bars: 4 μm. **(L)** Synaptic $GABA_AR$ α1 intensities and areas as judged by SV2 colocalization are similar at muskelin depleted (−/−, 9.81±0.42 and 12.49±0.33) and WT dendrites (+/+, 11.91±0.50 and 13.08±0.42). **(M)** Extrasynaptic surface $GABA_AR$ α1 intensities and areas, as judged by SV2-negative sites, respectively. Both values are significantly increased at muskelin depleted (−/−, 20.46±0.79 and 27.25±0.95) as compared to WT dendrites (+/+, 9.62±0.49 and 12.28±0.70). **(N)** DAB signals detected by electron microscopy of hippocampal tissue. Muskelin immunoreactivity labels extrasynaptic invaginations at the plasma membrane. Scale bar: 0.1 μm. (**O–Q**) The integrity of synapses is normal upon muskelin depletion. (**O**) Analysis of the presynaptic marker SV2. Intensity: +/+, 4.62±0.24; −/−, 4.83±0.31. Number of puncta: +/+, 6.43±0.35; −/−, 6.83±0.47; n=53 per genotype from 3 experiments. (**P, Q**) Colocalization of PSD-95 (excitatory postsynaptic sites) and gephyrin (inhibitory postsynaptic sites), respectively, with synaptophysin (excitatory and inhibitory axon terminals) in neurons derived from WT (+/+) and muskelin KO (−/−) mice. Scale bar: 4 μm. (**Q**) Quantification from eight cultures per genotype. PSD-95/synaptophysin: +/+, 17.28±0.94, n=85; −/−, 16.16±1.16, n=82. Gephyrin/synaptophysin: +/+, 20.52±1.01, n=79; −/−, 20.70±1.12, n=83. The Student's t test (***p<0.001; **p<0.01; *p<0.05) was used for statistical analysis. Data are represented as mean±SEM.

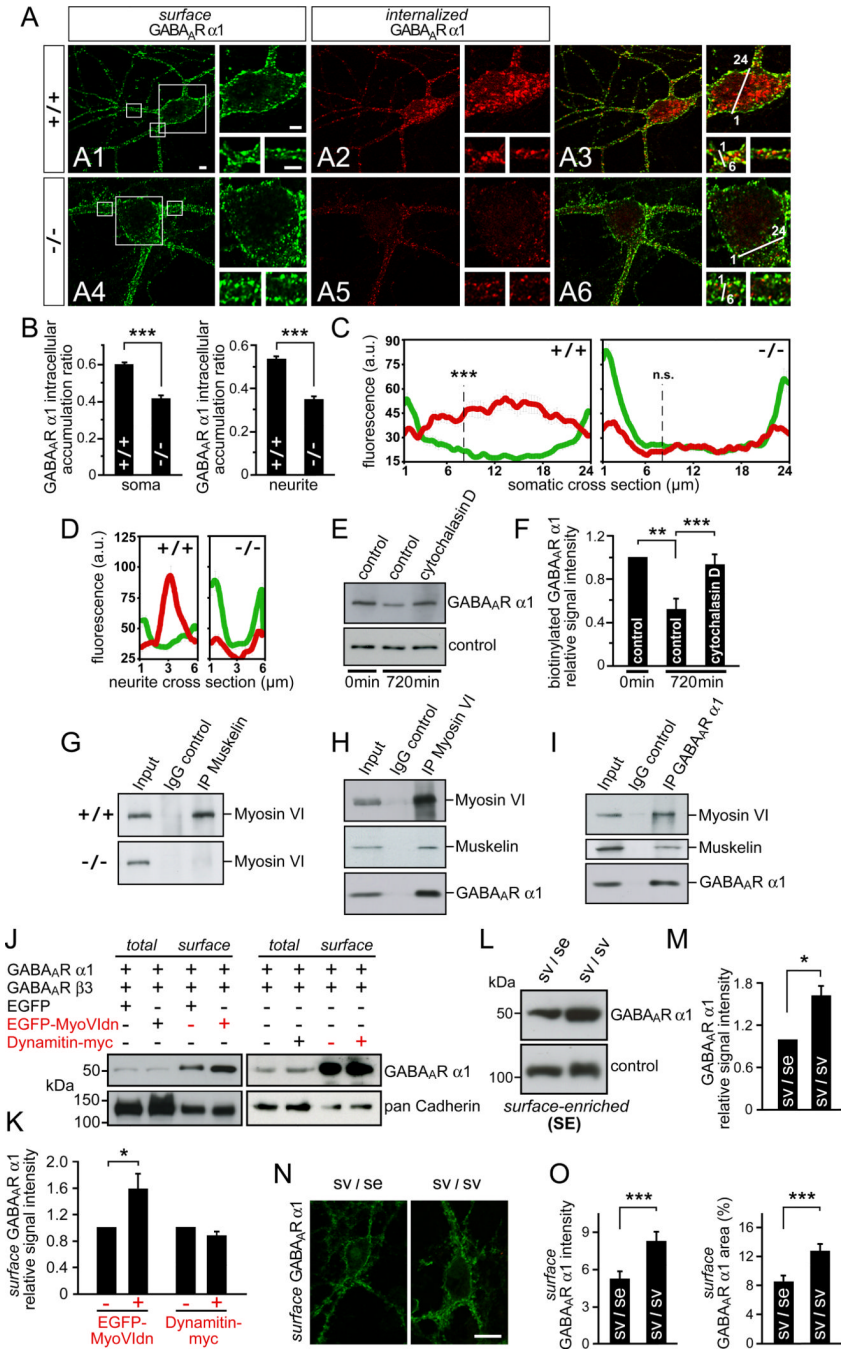

Figure 4. Muskelin-myosin VI interactions facilitate F-actin dependent GABA$_A$R α1 internalization in WT but not in muskelin and myosin VI mutant mice

(A–D) Receptor internalization assay in living neurons with labeling of surface GABA$_A$R α1. After an internalization period of 2h, remaining surface receptors stain green (A1, A4), internalized receptors stain red (A2, A5). Merged views appear in panels (A3) and (A6). Muskelin depleted neurons (−/−, A4–6) show less internalized receptors than WT neurons (+/+, A1–3) (n=48 cells from three cultures of each genotype). Boxed regions at higher magnifications, scale bars: 6 μm. **(B)** Significantly reduced GABA$_A$R α1 internalization rates at muskelin depleted (−/−, 0.42±0.01 and 0.35±0.01) as compared to WT somata and neurites (+/+, 0.60±0.01 and 0.54±0.01). (**C, D**) Quantitative line-scan analyses of

fluorescence intensities over cross-sections as indicated by white lines in panels (A3) and (A4). Fluorescence of internalized receptors (red) peak in the middle of somata (C) and neurites (D) in WT (+/+) but not in muskelin depleted (−/−) neurons. Remaining surface receptors (green) peak at cell boundaries in WT (+/+) neurons and display higher fluorescent peaks upon muskelin depletion (−/−), reflecting an increase in surface receptors (compare with Figure 3A–D). **(E, F)** Biotinylation of surface $GABA_AR$ α1 (time point 0 min) followed by analysis of receptor loss in cultured hippocampal neurons (n=8). **(F)** Significant loss of biotinylated $GABA_AR$ α1 after 720 min (0.52±0.09) as compared to time point 0 min (set to 1). Cytochalasin D significantly reverses this loss (0.93±0.10), indicating that receptor internalization requires intact F-actin. Control: actin detection. **(G–I)** Co-IPs from whole brain lysate in the presence of detergent (Triton-X-100). **(G)** Muskelin-specific antibodies coprecipitate myosin VI from WT (+/+) but not muskelin KO (−/−) derived lysates **(H–I)** Co-IPs with either myosin VI or $GABA_AR$ α1-specific antibodies reveal association of myosin VI and muskelin with $GABA_AR$ α1. **(J, K)** Surface $GABA_AR$ α1 biotinylation upon $GABA_AR$ β3 coexpression to achieve receptor surface localization in HEK293 cells. Control: Pan-Cadherin detection. Coexpression of a dominant-negative myosin VI peptide EGFP-MyoVIdn (n=8) causes significantly increased surface $GABA_AR$ α1 levels (1.58±0.20) as compared to EGFP coexpression (set to 1). Coexpression of the dynein inhibitor dynamitin-myc does not alter surface $GABA_AR$ α1 levels (0.86±0.05, n=4). (**L–O**) Increased $GABA_AR$ α1 levels at the neuronal cell surface of Snell`s waltzer mutant mice (sv/sv) lacking myosin VI. (**L, M**) $GABA_AR$ α1 levels at surface-enriched (SE) brain lysates from control (sv/se) and mutant mice (sv/sv) (sv/se: set to 1; sv/sv 1.64±0.13, n=3). (**N, O**) Surface $GABA_AR$ α1 immunostainings of hippocampal neurons. Dendritic $GABA_AR$ α1 intensities (left graph) and areas (right graph) are significantly increased in myosin VI depleted (sv/sv, 8.35±0.65 and 12.70±0.92) as compared to control neurons (sv/se, 5.35±0.62 and 8.50±0.72, n=43 sv/se; n=41 sv/sv cells from three cultures per genotype). The Student's t test (***$p<0.001$; **$p<0.01$; *$p<0.05$) was used for statistical analysis. Data are represented as mean±SEM.

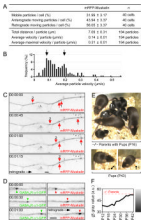

Figure 5. Coat color dilution of muskelin KO mice and muskelin/ $GABA_AR$ α1 cotransport

(A) Summary of muskelin motility parameters. Particles are highly mobile with characteristics similar to active retrograde motor protein transport. Data are represented as mean±SEM aquired from >8 hippocampal cultures (n as indicated). (**B**) The frequency of average muskelin particle velocities peaks at two distinct values (arrows). This observation might reflect an association of muskelin with two individual transport complexes, characterized by unique motility parameters. (**C**) Live imaging using DIV 10–14 cultured hippocampal neurons. Time-lapse video microscopy detects transport of mRFP-muskelin fusion particles. Particles 1 and 2 represent examples of retrogradely moving transport packets along a neurite over time. The arrow indicates an immobile reference particle. Scale bar: 14 μm. **(D)** Retrograde cotransport of colocalized $GABA_AR$ α1-GFP (left column) and mRFP-muskelin (right column) fusion particles along neurite processes. Scale bar: 14 μm. **(E)** Muskelin KO mice develop a dilute coat color. Homozygous (−/−) parents and their pups are shown. (−/−) pups initially have a black fur (P16), developing into a brighter fur over time (parents, pups P43). Close-up images of older pups are below (male and female). **(F)** Average gray values over multiple animals and time points. Right bar: light and dark color code. Around P43 the coat color change is complete with average gray values of 52.07±1.96 as compared to 38.35±2.63 at stage P12 (n=4). Data are represented as mean ±SEM.

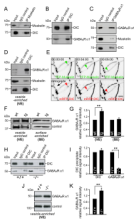

Figure 6. Dynein-driven, retrograde transport complex containing muskelin and $GABA_AR$ α1

(A–D) Co-IP analysis from whole brain lysates in the presence of detergent (Triton-X-100). Dynein is represented by its essential subunit dynein intermediate chain (DIC). **(A)** Dynein coprecipitates with muskelin. **(B)** $GABA_AR$ α1 coprecipitates with dynein. **(C)** Dynein and muskelin coprecipitate with $GABA_AR$ α1. **(D)** Using vesicle-enriched brain lysate fractions (VE), $GABA_AR$ α1 and muskelin coprecipitate with dynein. **(E)** Live imaging using DIV 10–14 cultured hippocampal neurons detects retrograde cotransport of colocalized YFP-muskelin (green) and mRFP-DIC (red) fusion particles across neurite processes. Scale bar: 20 μm. **(F, G)** Comparison of $GABA_AR$ α1 levels in vesicle- or surface-enriched brain lysate fractions from WT or transgenic mice (tg) overexpressing the dynein inhibitor dynamitin. Control: Actin detection. Loss of dynein transport (tg) significantly accumulates $GABA_AR$ α1 in vesicle-enriched fractions (VE, 1.54±0.10) as compared to WT set to 1 but does not alter $GABA_AR$ α1 levels in surface-enriched fractions (SE, 1.05±0.07), WT set to 1 (n=3). **(H, I)** DIC-specific antibodies coprecipitate $GABA_AR$ α1 from WT-derived brain lysates (+/+) set to 1. Upon muskelin depletion (−/−), $GABA_AR$ α1 coprecipitation is significantly reduced (0.25±0.02), indicating a requirement of muskelin for dynein/$GABA_AR$ α1 complex formation (n=3). $GABA_AR$ α1 coprecipitation was normalized to DIC precipitation (−/− 1.09±0.08 versus +/+ set to 1). **(J, K)** Similar as in absence of dynein function, depletion of muskelin causes $GABA_AR$ α1 to significantly accumulate in vesicle-enriched brain lysate (VE) fractions (−/−, 1.52±0.14) as compared to WT fractions (+/+, set to 1). Control: γ-Adaptin detection (n=7). Data are represented as mean±SEM. The Student's t test (**$p<0.01$) was used for statistical analysis.

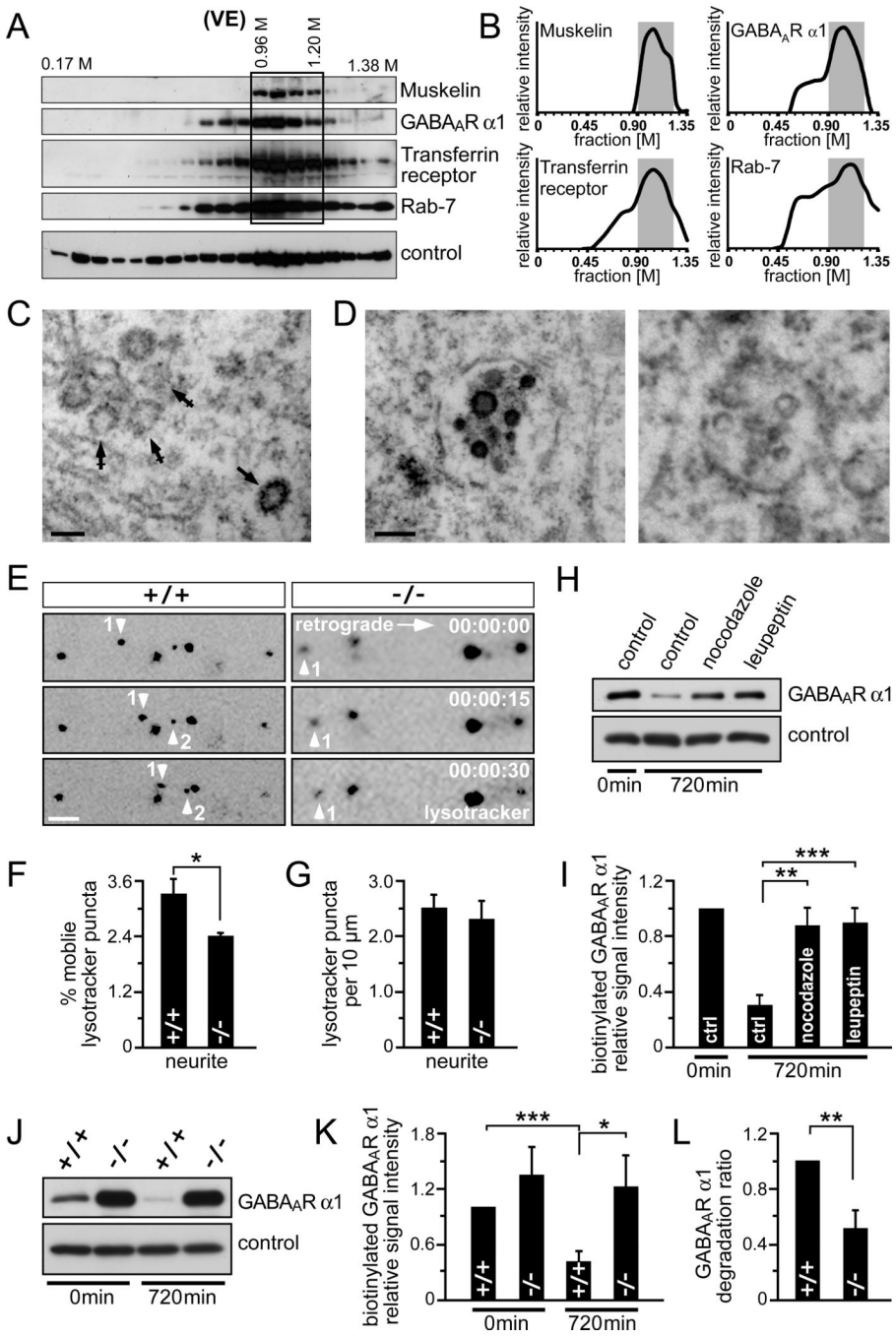

Figure 7. Muskelin facilitates degradation of $GABA_AR$ α1

(**A, B**) Sucrose gradient centrifugation of vesicle-enriched brain lysate (VE) fractions. $GABA_AR$ α1 and muskelin-containing vesicles cofractionate with transferrin receptor and Rab-7 containing endosomes (n=3). Control: NSF detection. (**C, D**) DAB signals detected by electron microscopy of hippocampal tissue. Muskelin immunoreactivity labels individual (C, arrow), but not all (crossed arrows) small vesicles. In addition, individual (D, left), but not all (right) multivesicular bodies and/or late endosomes stain positive for muskelin. Scale bar = 0.15 µm. **(E–G)** Late endosomes and lysosomes were labeled with LysoTracker and recorded live in cultured hippocampal neurons. Particles 1 and 2 are examples of retrogradely moving organelles along neurites over time (n=3 cultures of each genotype, 31

cells for +/+ and 25 for −/−). Scale bar: 14 μm. **(F)** Muskelin depletion significantly reduces mobility of LysoTracker puncta (−/−, 2.41±0.04), as compared to WT neurites (+/+, 3,33±0.30). **(G)** There are similar numbers of LysoTracker puncta in WT (+/+, 2,53±0.21) and muskelin KO (−/−, 2.33±0.32) neurites. **(H–L)** Receptor degradation assay tracking the loss of biotinylated $GABA_AR$ α1 over 720 min of internalization and degradation using cultured hippocampal neurons. **(I)** Significant less biotinylated $GABA_AR$ α1 after 720 min (0.31±0.07) as compared to surface receptor amounts at time point 0 (set to 1). The lysosome blocker leupeptin (0.88±0.12) and the microtubule-depolymerizing agent nocodazole (0.89±0.10) significantly reverse this loss, indicating that receptor degradation requires intact microtubules (n=4). Control: Actin detection. **(J, K)** $GABA_AR$ α1 surface levels at time point 0 are increased in muskelin KO (−/−, 1.34±0.26) as compared to WT neurons (+/+, set to 1), reflecting a surface $GABA_AR$ α1 accumulation upon muskelin depletion (compare Figure 3, A–D). The loss of biotinylated $GABA_AR$ α1 observed in WT neurons after 720 min (+/+, 0.42±0.10) is not observed upon muskelin depletion (−/−, 1.22±0.30) (n=8). Control: Actin detection **(L)** Ratios of $GABA_AR$ α1 degradation as defined by the quotient of 0 and 720 min are reduced in absence of muskelin (−/−, 0.52±0.12), as compared to WT (+/+, set to 1). Data are represented as mean±SEM. The Student's t test (***$p<0.001$; **$p<0.01$; *$p<0.05$) was used for statistical analysis.

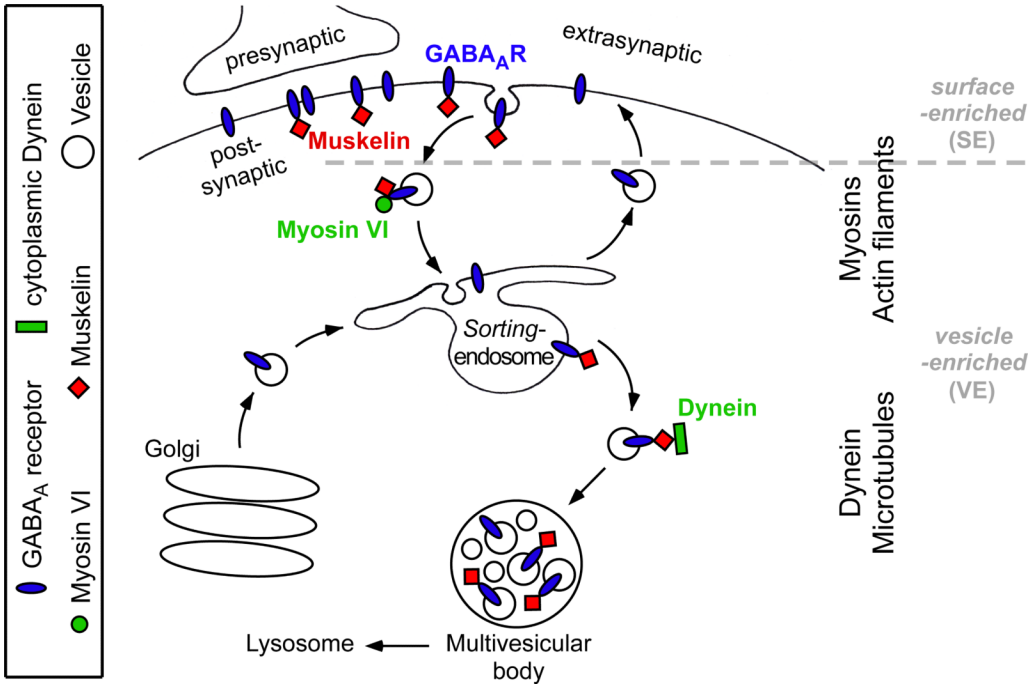

Figure 8.

Model of muskelin functions. The retrograde trafficking of GABA$_A$Rs is of broad interest in synaptic plasticity and network oscillations; however, the drivers of retrograde GABA$_A$R trafficking have remained unknown. A Summary is shown of the molecular basis of GABA$_A$R transport that undergoes, similar to other transmembrane proteins (Traer et al., 2007), two subsequent steps. Step1: internalization from the surface membrane towards sorting endosomes. Internalization occurs at the cellular cortex, which is rich in F-actin and is thought to involve myosin motors for active cargo transport (Osterweil et al., 2005). Step2: translocation from sorting endosomes to either recycling or degradation pathways. This step is known to employ microtubule-based motors, including dynein (Traer et al., 2007) for cargo transfer towards the cellular interior. The question of how specific cargoes can physically switch between and are guided through different transport systems, is barely understood. The data in this study identify muskelin in physical association with GABA$_A$Rs at cell surface as well as intracellular vesicle compartments (Fig.1, 7). Moreover, they show a functional association of muskelin with myosin VI- and dynein motor complexes (Fig.4, 6), acting at two different types of cytoskeletal tracks. In the absence of functional myosin VI motor activity or without intact F-actin, GABA$_A$Rs accumulate at the surface membrane, only. Hence, inhibition of dynein function and disruption of the microtuble network only leads to enrichment of GABA$_A$Rs in vesicle compartments, but not at the cell surface. The genetic KO of muskelin, in contrast, causes accumulation within both compartments by i), reducing receptor cell surface removal and ii), lowering the rate of lysosomal receptor degradation (Fig.3, 4, 6, 7). The dilute coat color phenotype of muskelin KO mice, strongly suggests that muskelin acts similarly on transport systems beyond neurons (Fig.5). Together, our data propose a novel concept in neuronal cell biology: common trafficking factors that functionally interconnect specific cargoes to subsequently traverse different cytoskeletal track systems via active motor protein transport.